BIOCHEMISTRY
including biophysical chemistry & molecular biology
Article

Biochemistry **2010,** *49,* 2903–2917 2903
DOI: 10.1021/bi901963e

Modular Structure of Smooth Muscle Myosin Light Chain Kinase: Hydrodynamic Modeling and Functional Implications[†]

Yasuko Mabuchi,[‡] Katsuhide Mabuchi, Walter F. Stafford, and Zenon Grabarek*

Boston Biomedical Research Institute, Watertown, Massachusetts 02472. [‡]*Current address: Pfizer, Biotherapeutics R&D, 1 Burtt Rd., Andover, MA 01810.*

Received November 13, 2009; Revised Manuscript Received February 19, 2010

ABSTRACT: Smooth muscle myosin light chain kinase (smMLCK) is a calcium−calmodulin complex-dependent enzyme that activates contraction of smooth muscle. The polypeptide chain of rabbit uterine smMLCK (Swiss-Prot entry P29294) contains the catalytic/regulatory domain, three immunoglobulin-related motifs (Ig), one fibronectin-related motif (Fn3), a repetitive, proline-rich segment (PEVK), and, at the N-terminus, a unique F-actin-binding domain. We have evaluated the spatial arrangement of these domains in a recombinant 125 kDa full-length smMLCK and its two catalytically active C-terminal fragments (77 kDa, residues 461−1147, and 61 kDa, residues 461−1002). Electron microscopic images of smMLCK cross-linked to F-actin show particles at variable distances (11−55 nm) from the filament, suggesting that a well-structured C-terminal segment of smMLCK is connected to the actin-binding domain by a long, flexible tether. We have used structural homology and molecular dynamics methods to construct various all-atom representation models of smMLCK and its two fragments. The theoretical sedimentation coefficients computed with HYDROPRO were compared with those determined by sedimentation velocity. We found agreement between the predicted and observed sedimentation coefficients for models in which the independently folded catalytic domain, Fn3, and Ig domains are aligned consecutively on the long axis of the molecule. The PEVK segment is modeled as an extensible linker that enables smMLCK to remain bound to F-actin and simultaneously activate the myosin heads of adjacent myosin filaments at a distance of ≥40 nm. The structural properties of smMLCK may contribute to the elasticity of smooth muscle cells.

The primary pathway for the regulation of contraction in smooth muscles involves the calcium−calmodulin complex-dependent activation of myosin light chain kinase (MLCK). Upon stimulation of a smooth muscle cell, the level of Ca^{2+} in the cytoplasm is transiently elevated due to influx from the extracellular fluid or from intracellular stores via the action of inositol 1,4,5-trisphosphate. The Ca^{2+}−CaM[1] complex binds to and activates MLCK, which in turn phosphorylates the 20 kDa regulatory light chain of myosin (LC20) at Ser19 and Thr18, leading to the activation of myosin ATPase by actin and to muscle contraction.

The phosphotransferase catalytic function of MLCK is localized in an ∼300-residue (∼35 kDa) structurally conserved domain (*1*, *2*) that exhibits a high degree of sequence similarity to other protein kinases (*3*). The function of this domain is regulated by the intrasteric inhibition involving a pseudosubstrate segment located at the C-terminus of the domain. The inhibition is released when the Ca^{2+}−CaM complex binds to the adjacent specific CaM binding site (*4*−*7*). The polypeptide chain of rabbit skeletal MLCK (Swiss-Prot entry P07313) contains 607 residues (*8*), which is twice as long as the minimum required for catalytic function. Much longer are the polypeptide chains of smooth muscle MLCK, e.g., chicken gizzard (Swiss-Prot entry P11799-2) (*9*) or rabbit uterine MLCK (Swiss-Prot entry P29294) (*10*), which contain 972 and 1147 amino acids, respectively. The largest known MLCK is the 210 kDa non-muscle isoform (e.g., Swiss-Prot entries Q15746-1 and P11799-1) (for a review, see ref *7*). The functional significance of such complex structures is unclear.

Analysis of the amino acid sequence of rabbit uterine MLCK indicates several distinct domains in the 1147-amino acid polypeptide chain of this protein (*10*). It has been established that smMLCK binds both F-actin (*11*) and unphosphorylated smooth muscle myosin with micromolar K_d values (*12*). The F-actin-binding site has been localized at the N-terminus of smMLCK (*13*, *14*) and shown to involve three DFRxxL motifs (*15*). The three-dimensional (3D) reconstructions of F-actin decorated with the N-terminal 147-residue fragment of smMLCK showed MLCK density on the extreme periphery of subdomain 1 of each actin monomer forming a bridge to subdomain 4 of the azimuthally adjacent actin (*16*). This unique location enables MLCK to bind to actin without interfering with the binding of any other key actin-binding proteins, including myosin, tropomyosin, caldesmon, and calponin. Next to the actin-binding domain is a segment containing 16 repeats of a proline-rich 12-residue motif, TLKPV(G,A)N(A,I,T)KPAE (*10*). A similar sequence occurs in smooth muscle MLCK from bovine

[†]This work was supported by National Institutes of Health Grants AR-41637 and HL-91162.

*To whom correspondence should be addressed: Boston Biomedical Research Institute, 64 Grove St., Watertown, MA 02472-2829. E-mail: Grabarek@BBRI.org. Telephone: (617) 658-7805. Fax: (617) 972-1753.

[1]Abbreviations: smMLCK, smooth muscle myosin light chain kinase; 61k-MLCK and 77k-MLCK, recombinant fragments of rabbit smooth muscle myosin light chain kinase containing residues 461−1002 and 461−1147, respectively; CaM, calmodulin; MD, molecular dynamics.

Published on Web 03/02/2010

stomach and a shorter one in MLCK isolated from human brain. This segment is absent from chicken gizzard and from skeletal muscle MLCK. This region has been termed the PEVK region by analogy to the Pro-, Glu-, Val-, and Lys-rich segment of the giant protein titin (*17*−*19*). Adjacent to the repetitive segment is a 90-residue immunoglobulin-related domain (Ig1) followed by a linker that is readily cleaved by proteolytic enzymes (*20*, *21*). Further downstream is another Ig domain (Ig2) and a fibronectin type III related motif (Fn3). The catalytic and regulatory domains that follow the Ig2−Fn3 tandem are by far the most studied parts of MLCK (for reviews, see refs *7* and *22*). Finally, at the C-terminus is one more Ig motif (Ig3) terminated with a stretch of Glu residues (polyE). The 154-residue C-terminal segment of smMLCK containing the Ig3 domain is also expressed in a manner independent of the full-length MLCK and is termed telokin (*23*) or kinase-related protein (KRP) (*24*). Telokin was found to promote filament formation of unphosphorylated myosin in the presence of ATP presumably through its binding to the head−tail junction of myosin (*25*). Telokin was found to decrease the K_m but not the V_{max} of myosin phosphorylation by MLCK (*25*). It appears that the C-terminal extension of smMLCK corresponding to telokin also interacts with myosin, but the significance of this interaction for the catalytic activity of MLCK is not clear. Telokin is the only part of smMLCK whose high-resolution structure has been determined (*26*). The presence of the specific actin and myosin binding sites at the extreme termini of the polypeptide chain suggests that in smooth muscle smMLCK might interact simultaneously with both thin and thick filaments. Stull et al. considered such a possibility in their 1998 review article (*27*). They pointed out that if the independently folded Ig, Fn3, and catalytic domains of smMLCK are arranged in a linear fashion, while the remaining segments are in an extended conformation, the molecule could span more than 600 Å and readily bridge the thick and thin filaments in smooth muscle cells. This hypothesis is consistent with the elongated shape in solution of skeletal and turkey gizzard MLCK as previously determined by analytical ultracentrifugation (*2*, *28*, *29*). It is also consistent with the observation that smMLCK is virtually immobilized in cultured smooth muscle cells (*30*). However, the postulated linear arrangement of the domains, the flexibility of the unstructured segments, and their contribution to the overall shape and hydrodynamic properties of smMLCK have not been rigorously evaluated.

In these studies, we have used electron microscopy, analytical ultracentrifugation, structural homology, and hydrodynamic modeling to obtain information about molecular shape and domain arrangement in recombinant rabbit smooth muscle MLCK and its two catalytically active fragments. We have found that the hydrodynamic properties of smMLCK are consistent with a modular structure in which the C-terminal part of the molecule is built of well-structured domains arranged in a linear fashion. This part of smMLCK is connected to the N-terminal actin-binding site through a flexible and extensible segment, the PEVK region. The structural properties of smMLCK appear to facilitate the preferential activation of those myosin heads that are in contact with F-actin filaments and to contribute to the elasticity of smooth muscle cells.

MATERIALS AND METHODS

Cloning and Overexpression of the Rabbit Uterine MLCK in Insect Cells. We have overexpressed the full-length rabbit uterine smooth muscle MLCK in insect cells. A 3.4 kb cDNA comprising the coding region of smMLCK was constructed from two overlapping cDNA fragments (N-terminal 2.48 kb and C-terminal 1.52 kb in pGem vector) generously provided by P. J. Gallagher and J. T. Stull. After removal of the overlapping sequence and ligation of the complementary fragments, the full-length cDNA was subcloned into baculovirus transfer vector pBlueBac4 (Invitrogen) at BamHI and KpnI sites and cotransfected into SF9 insect cells using a BAC-N-Blue (linear AcMVNPV DNA) transfection kit (Invitrogen). The presence of smMLCK DNA was confirmed by PCR analysis of viral DNA, and the expression of smMLCK was confirmed by Western blotting. After propagation of a high-titer viral stock, 500 mL of a High Five insect cell suspension culture was infected with 10 mL of the viral stock, and after being cultured at 28 °C for 48 h, cells were harvested by centrifugation. The cell pellet was suspended in 30 mL of a solution containing 50 mM NaCl, 50 mM $MgCl_2$, 20 mM MOPS (pH 7.0), 0.5 mM EGTA, 0.2 mM 4-(2-aminoethyl)benzenesulfonyl fluoride hydrochloride (AEBSF), 1 mM DTT, 10% glycerol, and 0.04 mM leupeptin. MLCK was extracted by the freezing and thawing of the cell suspension three times. After centrifugation of the extract at 100000*g* for 30 min, clear supernatant was applied onto a DEAE-Sepharose CL 6B column equilibrated with a solution containing 50 mM NaCl, 30 mM $MgCl_2$, 20 mM MOPS (pH 7.0), 0.5 mM EGTA, 1 mM DTT, and 0.2 mM AEBSF. Protein was eluted with a linear gradient from 0.05 to 0.45 M NaCl. The peak containing MLCK was collected and further purified with the use of a CaM affinity column. The yield of MLCK was ~10 mg. The enzymatic activity of MLCK was confirmed by myosin LC20 electrophoretic mobility shift assay.

In addition to the full-length MLCK, we have generated and expressed in baculovirus its two fragments: a 77 kDa C-terminal fragment comprising residues 461−1147 (77k-MLCK) and a 61 kDa fragment (residues 461−1002) containing the catalytic/regulatory domain and the Ig2 and Fn3 motifs on the N-terminal side of the catalytic domain. This construct corresponds to the stable MLCK fragment that is generated by limited proteolysis from the full-length chicken gizzard MLCK (*21*). 77k-MLCK and 61k-MLCK were expressed and purified in a manner similar to that of the full-length protein.

Other Proteins. Actin from rabbit skeletal muscle was obtained from acetone-dried muscle powder essentially according to the method of Spudich and Watt (*31*), except for the 3 day dialysis step which was shortened to overnight dialysis with a single change of buffer. Recombinant human calmodulin was obtained as previously described (*32*).

Analytical Ultracentrifugation. Sedimentation velocity experiments were conducted on a Beckman Instruments Optima XL-I analytical ultracentrifuge equipped with a real-time video-based data acquisition system and Rayleigh optics. The cells were equipped with sapphire windows and 12 mm charcoal-filled Epon centerpieces. Sedimentation velocity patterns were acquired every 8 s. Apparent sedimentation coefficient distribution patterns were computed by the time derivative method (*33*−*35*). All protein solutions were dialyzed against their respective buffers, and dialysate was used for all dilutions. Molecular masses were computed from sedimentation velocity profiles using SEDANAL, which employs a nonlinear least-squares curve fitting algorithm to fit data to solutions of the differential equation (the Lamm equation) describing sedimentation. Fits were conducted on time difference data to remove the

time-independent systematic baseline components according to Stafford and Sherwood (*36*). Values of s and D obtained from the fitting procedure were substituted into the Svedberg equation to yield the molar mass of the protein, M_2:

$$M_2 = \frac{RT}{1 - v_2\rho} \frac{s^{o}_{20,w}}{D^{o}_{20,w}}$$

where ρ is the density of the buffer and v_2 is the partial specific volume of the protein. Values of the partial specific volume, v_2, were computed from the amino acid sequence using the consensus partial volumes of Perkins (*37*). The axial ratios of the corresponding ellipsoids of revolution were calculated using Perrin's equation for a prolate ellipsoid having semiaxes a, b, b (cf. eq 19-14 of ref *38*):

$$\frac{f}{f_o} = \frac{\left(1 - \frac{b^2}{a^2}\right)^{1/2}}{\left(\frac{b}{a}\right)^{2/3} \ln\left[\frac{1 + \left(1 - \frac{b^2}{a^2}\right)^{1/2}}{\frac{b}{a}}\right]}$$

where f is the observed frictional coefficient and is computed from the experimentally observed values of M_2 and $s^{o}_{20,w}$ as follows:

$$f = \frac{M_2(1 - v_2\rho)}{Ns^{o}_{20,w}}$$

and f_o is the frictional coefficient of a sphere having the same mass and hydration as the protein and is given by

$$f_o = 6\pi\eta_o\left[\frac{3M_2(v_2 + \delta_1 v_1^{o})}{4N\pi}\right]^{1/3}$$

where η_o is the viscosity of water at 20 °C, δ_1 is the hydration of the protein in units of grams of water per gram of protein, v_1^{o} is the specific volume of pure water, and N is Avogadro's number. Values of hydration, δ_1, were computed from the data of Kuntz and Kauzman (*39*). The dimensions of a protein molecule were obtained by equating its hydrated volume (V) to the volume of a corresponding prolate ellipsoid:

$$V = \frac{4}{3}\pi ab^2 = \frac{M_2(v_2 + \delta_1 v_1^{o})}{N}$$

and using the axial ratio (b/a) obtained from Perrin's equation included above.

Rotary Shadowing Electron Microscopy. Samples of smMLCK or its fragments were diluted to a concentration of 4 nM in a solution containing 0.5 M ammonium acetate, 30% glycerol, 10 mM NaCl, and 3 mM $MgCl_2$. smMLCK cross-linked to F-actin (5.7 μM with respect to the actin monomer) was diluted 5-fold in F-buffer and centrifuged at 3000g for 10 min, and then the supernatant was further diluted in a solution containing 0.5 M ammonium acetate (pH 7.0) and 30% glycerol. The purpose of the centrifugation was to remove aggregates, and the high salt concentration was used to dissociate any un-cross-linked MLCK that might remain bound to F-actin during specimen preparation. The protein samples were adsorbed onto a freshly cleaved mica sheet, then stabilized by a treatment with uranyl acetate (*40*), and processed for rotary shadowing as previously described (*41*). EM specimens were observed under a Philips 300A electron microscope at 60 kV.

Zero-Length Cross-Linking of smMLCK to F-Actin. smMLCK was cross-linked to F-actin with the use of our EDC-NHS two-step zero-length cross-linking procedure (*42*). In the activation step, F-actin (1 mg/mL) in a solution containing 0.1 M NaCl, 2 mM $MgCl_2$, 0.2 mM ATP, 0.2 mM $CaCl_2$, and 20 mM MOPS (pH 7.0) was incubated with 1 mM 1-ethyl-3-[(dimethylamino)propyl]carbodiimide (EDC) and 2 mM *N*-hydroxysuccinimide (NHS) for 15 min followed by the addition of 5 mM β-mercaptoethanol to block the excess of EDC. Then, smMLCK was added from the stock solution in 0.1 M NaCl, 2 mM $MgCl_2$, and 20 mM MOPS (pH 7.0) to make the final molar ratio of smMLCK to actin equal 1:3. The solution was incubated for 1 h at room temperature. Cross-linking was verified by sodium dodecyl sulfate−polyacrylamide gel electrophoresis. The cross-linked proteins were analyzed by rotary shadowing electron microscopy.

Molecular Modeling. For modeling the catalytic, Ig, and Fn3 domains, we have used the Swiss Model server (http://swissmodel.expasy.org/SWISS-MODEL.html) in automatic and interactive modes facilitated by the Swiss PDB viewer program (*43*−*47*). Progressively more complex structures (61k-MLCK, 77k-MLC, and smMLCK) were built manually from individual domains with O (*48*). The structure of each construct was energy minimized and subjected to molecular dynamics simulation in vacuo using CNS (*49*). The N-terminal 99-residue actin binding region and the short interdomain linker segments were first modeled in the extended conformation and then subjected to molecular dynamics simulation for 100 ps, which caused the extended chain to collapse into a random and relatively compact form. The 16 × 12 tandem repeat (residues 100−288) was modeled initially as a polyproline type II helix (ϕ = −75°, ψ = 145°, and ω = 180°) and also subjected to molecular dynamics for 50, 200, and 300 ps, leading to different levels of structure collapse and randomization. These partially randomized structures were used to construct models of the full-length smMLCK. The theoretical sedimentation coefficients for the modeled proteins were calculated with HYDROPRO (*50*) using the full set of atomic coordinates as input for each model.

RESULTS

Recombinant smMLCK and Its C-Terminal Catalytically Active Fragments. In this study, we have used purified recombinant rabbit uterine MLCK overexpressed in insect cells with the use of a baculovirus expression system. In addition to the full-length smMLCK, we have also constructed two fragments comprising the C-terminal part of the molecule: 77k-MLCK (residues 461−1147) and 61k-MLCK (residues 461−1002) (Figure 1). 61k-MLCK corresponds approximately to the proteolysis resistant catalytically active core domain of smMLCK (*1*, *20*, *51*). It comprises the Ig2−Fn3 tandem and the kinase/regulatory domain, including the autoinhibitory segment and the CaM binding site. 77k-MLCK contains also the telokin region (Ig3) and the C-terminal poly-Glu segment. An illustration of typical purification steps and the quality of the obtained protein preparations is shown in Figure 2. All three proteins have the full Ca^{2+}−CaM complex-regulated kinase activity with respect to both smooth muscle myosin and isolated regulatory light chain LC20. Turnover rates measured at a low temperature (4 °C) and a

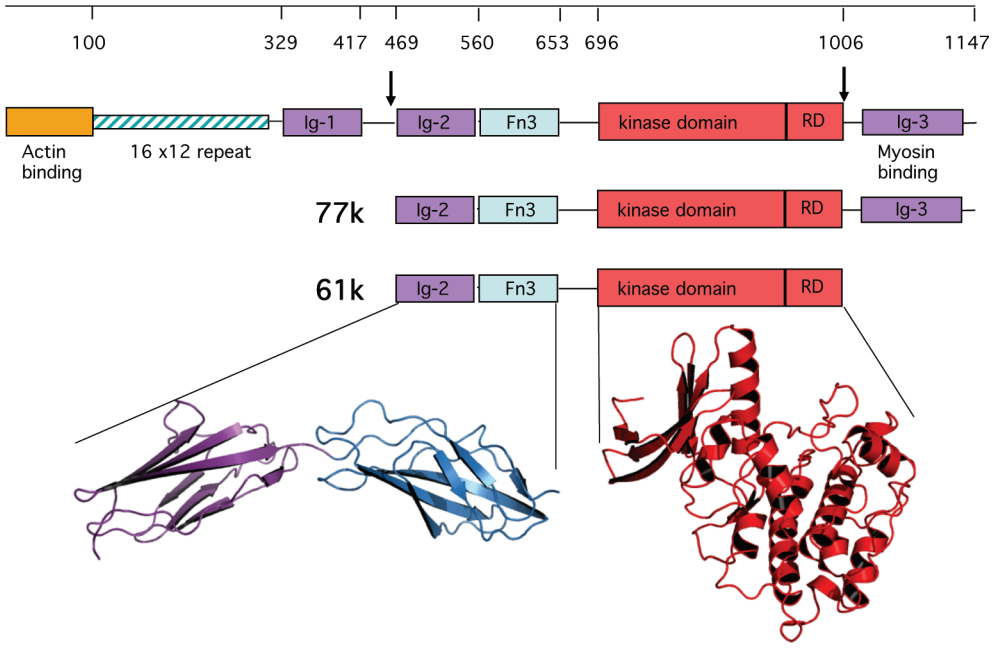

FIGURE 1: Structural domains of smMLCK. Domain definition based on refs *9* and *10*. The central segment marked by the arrows corresponds to the trypsin resistant fragment of smMLCK, which is equivalent to the recombinant 61k-MLCK used in this study. This fragment comprises the Ig2−Fn3 tandem and the catalytic/regulatory domain. 77k-MLCK has the same N-terminus as the 61k fragment and extends to the C-terminus of smMLCK to include the Ig3 (telokin) region. The atomic models of the Ig2−Fn3 tandem and the catalytic/regulatory domain obtained by homology modeling are shown in ribbon representation (see the text and Table 2 for details).

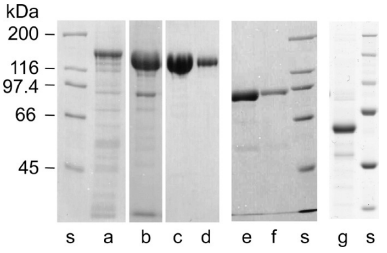

FIGURE 2: Purification of the full-length mammalian smMLCK and its C-terminal active fragments overexpressed in insect cells. Representative examples of electrophoresis on a sodium dodecyl sulfate−polyacrylamide gel (8%) of smMLCK samples at various steps of purification are shown: (a) extract of soluble proteins from High Five cells expressing smMLCK, (b) peak fraction from a DEAE-Sepharose CL 6B column, and (c and d) smMLCK eluted in EGTA from a CaM affinity column (two different loads are shown). The 77k-MLCK (e and f) and 61k-MLCK (g) fragments of smMLCK were obtained with similar yields. A molecular mass standard (Bio-Rad) is shown for each preparation (s).

low substrate concentration (0.5 μM LC20) are 15.3, 22.0, and 10.0 min^{-1} for the full-length MLCK, 77k-MLCK, and 61k-MLCK, respectively.[2] These rates correspond to the extrapolated V_{max} values in the range of 10−25 μmol min^{-1} mg^{-1} [at 25 °C and an infinite substrate concentration, assuming K_d(LC20) = 10 μM], which is similar to the published values for smMLCK expressed in COS cells (*10*, *52*).

Electron Microscope Images of smMLCK Bound to F-Actin. We have examined the interaction of the full-length smMLCK with F-actin by rotary shadowing electron microscopy. To overcome the problem of dissociation of MLCK from F-actin during specimen preparation, we have cross-linked smMLCK to F-actin with the use of the two-step zero-length cross-linking procedure (*42*). In this method, one component of the protein complex is briefly activated with a water-soluble carbodiimide (EDC) in the presence of *N*-hydroxysuccinimide (NHS). This converts some exposed carboxyl groups into *N*-succinimidyl active esters, which can cross-link to nearby Lys side chains or hydrolyze back to the original carboxyls. The second protein component of the complex is added after the activation step is terminated by the addition of β-mercaptoethanol, which blocks the remaining EDC. The cross-linking occurs during the subsequent 1−2 h incubation. The advantage of this procedure is that only one component of the complex is exposed to the cross-linker, thus avoiding the possibility of intramolecular cross-linking of smMLCK. We found extensive smMLCK−actin cross-linking when F-actin was activated with EDC and NHS, whereas no cross-linking occurred when smMLCK was activated.

The F-actin-cross-linked smMLCK is visible in the rotary shadowing EM images as an array of elongated and often curved or oval-shaped objects positioned variable distances from the filament (Figure 3). Apparently, these objects are tethered to F-actin by a segment of the molecule that is too thin to be visualized by rotary shadowing. Clearly, the distribution of mass in smMLCK is not uniform. There is a long, thin, and flexible linker between the actin cross-linking site and the well-structured part of smMLCK. To assess the length of the linker region, we have measured the distances between the edge of the F-actin filament and the most distant visible parts of the cross-linked MLCK. The measured distances fall in a broad range of 11−55 nm, with an average distance of 28.3 ± 9.9 nm (n = 180). The distribution appears to be bimodal with a broad peak between 16 and 30 nm and a second peak at ~40 nm (Figure 4). Several reasons could account for such a broad range of observed lengths of F-actin-cross-linked smMLCK. First, the cross-linking may, in principle, involve nonspecific random interaction sites distributed along the polypeptide chain of MLCK. Although we have not verified this possibility, we can exclude the C-terminal

[2]A. Sobieszek and Z. Grabarek, unpublished data. The full account of these studies will be published elsewhere.

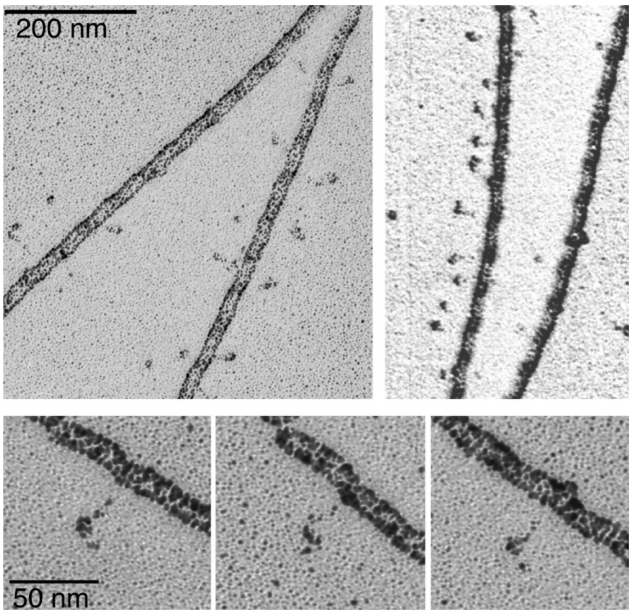

FIGURE 3: Rotary shadowing images of smMLCK zero-length cross-linked to F-actin. Note particles that appear to be tethered to the filament. The distance between these particles and the actin filament is highly variable.

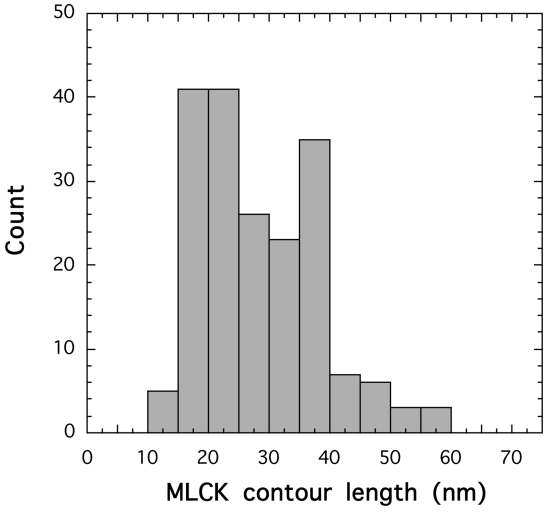

FIGURE 4: Contour length distribution of smMLCK cross-linked to F-actin. The length is measured from the edge of the actin filament to the most distant distinguishable parts of the tethered smMLCK. The distribution of distances is bimodal with a broad peak between 16 and 30 nm and a second peak at 40 nm. The width of the actin filament image is 15.9 ± 1.2 nm.

60% of the molecule as being potentially involved in the cross-linking, since the 77 kDa C-terminal fragment of MLCK does not cross-link to F-actin under the same conditions (data not shown). This observation suggests that the cross-linking requires a specific interaction site having a well-defined polarity of electrostatic contacts, i.e., F-actin contributing negatively charged groups. Thus, the cross-linking most likely involves the specific actin-binding site at the N-terminus of smMLCK identified by Smith et al. (*15*). The visible oval-shaped objects apparently represent the C-terminal part of smMLCK, including the catalytic domain. Second, the thickness of F-actin and the helical distribution of the binding sites on the actin monomers along the filament may contribute to the apparent length of the bound MLCK. The measured width of the F-actin filament in Figure 3 is 15.9 ± 1.2 nm; thus, a fully extended MLCK molecule attached at the distal side of the filament may appear up to 16 nm shorter than that attached to the proximal side. Third, it is impossible to assess whether a molecule extends from the filament in a perpendicular direction or other directions, since the linker is not visible. Thus, the measured distance from the filament may be shorter than the actual length of the molecule, if it extends at an angle with respect to the filament. Finally, the structural extensibility of the linker or other parts of smMLCK may contribute to the broad length distribution. Figure 3 also suggests that the distribution of smMLCK on actin may be nonrandom. Highly decorated filaments are visible next to segments that are free of MLCK. Also, when the filaments are highly decorated with the cross-linked MLCK, the spacing between the MLCK molecules appears to be rather uniform. The reasons for such a nonrandom distribution are not clear. In Figure 3, there are sections of F-actin that appear to have MLCK on only one side, while the opposing side is free of MLCK. We believe such an appearance is caused by the flow of solvent during specimen preparation, which orients tethered MLCK molecules on one side of the filament.

The rotary shadowing EM technique has been used previously to visualize chicken gizzard MLCK by Numata et al. (*53*). They reported that the molecule is flexible, since several distinct shapes can be distinguished, ranging from fully extended to highly compact structures. We have also used the rotary shadowing technique to visualize our recombinant rabbit smooth muscle MLCK (Figure 5) and found the results to be consistent with those of Numata et al. Images of smMLCK could be roughly subdivided into two classes: an extended conformation with a contour length of 36.4 ± 5.0 nm (standard deviation) and a compact conformation with a contour length of 23.9 ± 3.2 nm. The corresponding widths are 11.9 ± 1.5 and 14.8 ± 2.4 nm for the extended and compact conformations, respectively. The rotary shadowing images of 77k-MLCK (Figure 6) exhibited significantly less variability in shape than those of smMLCK. The majority of molecules were extended with an average contour length of 25.0 ± 2.9 nm and average width of 11.6 ± 1.9 nm. A comparison of rotary shadowing images of smMLCK alone, whether chicken gizzard or recombinant rabbit smooth muscle, with those of smMLCK cross-linked to F-actin suggests that the N- and C-terminal parts of the molecule have very different properties and only the latter is visible in rotary shadowing images.

It is instructive to compare the images of rabbit smMLCK cross-linked to F-actin (Figure 3) with those of gizzard MLCK cross-linked to the HMM part of myosin obtained by Numata et al. (*53*). In the latter case, MLCK is visible as a globular particle similar in size to the myosin heads and attached to the neck region of HMM. Clearly, the site of MLCK cross-linking to actin is very different from that involved in cross-linking to HMM. The former is located next to a flexible part of the molecule, while the latter is located at or next to a well-structured part of MLCK. This conclusion is consistent with the location of the respective binding sites at the extreme N- and C-termini of smMLCK, as determined from biochemical studies, and supports the view that the cross-linking involves the respective specific interaction sites.

Molecular Shape of smMLCK from Sedimentation Velocity. We have used sedimentation velocity to determine hydrodynamic parameters of smMLCK and its two C-terminal fragments, 77k-MLCK and 61k-MLCK. In view of the reported dimerization of chicken gizzard MLCK (*54*) that was modified by

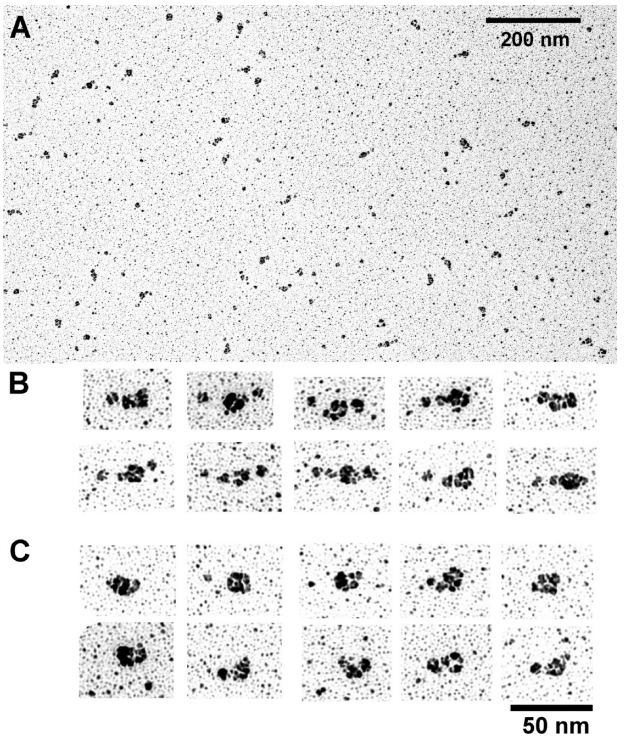

FIGURE 5: Rotary shadowing images of smMLCK. A low-magnification field (A) and ensembles of high-magnification images of single molecules in the extended (B) and compact (C) conformation are shown. The measured contour length for the extended conformation (L_e) is 36.4 ± 5.0 nm and for the compact conformation (L_c) is 23.9 ± 3.2 nm. The corresponding widths are 11.9 ± 1.5 nm (W_e) and 14.8 ± 2.4 nm (W_c).

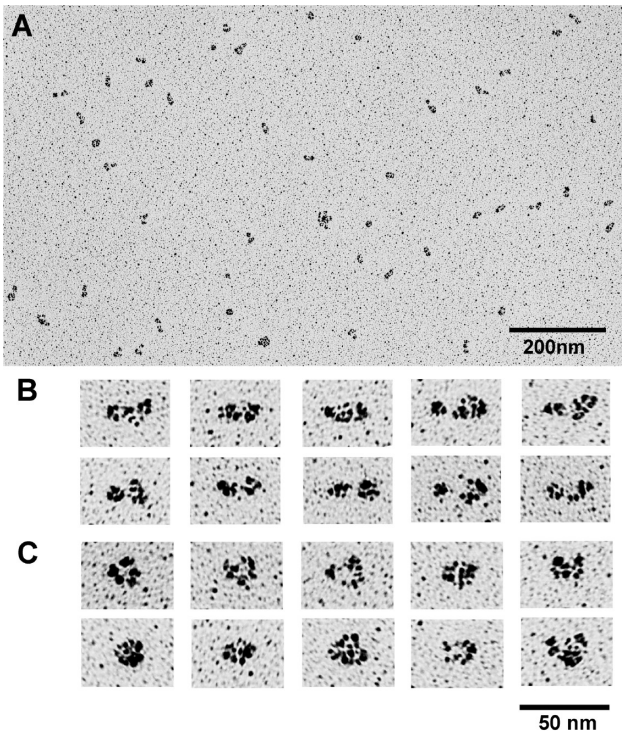

FIGURE 6: Rotary shadowing images of the 77k fragment of smMLCK. The low-magnification (A) and high-magnification (B and C) images are shown. The average contour lengths are 25.0 ± 2.9 nm (L_e) and 18.6 ± 2.0 nm (L_c), for the extended (B) and compact (C) conformations, respectively. The corresponding widths are 11.6 ± 1.9 nm (W_e) and 15.6 ± 1.8 nm (W_c).

the Ca^{2+}−CaM complex (*55*, *56*), we have tested the concentration dependence of the sedimentation velocity profile of smMLCK in the absence and presence of the Ca^{2+}−CaM complex. We find the sedimentation profile to be consistent with a monomeric state of the protein (Figure 7 and Table 1). Variation of concentration over a 10-fold range had no effect on the sedimentation coefficient (Figure 7a, dashed lines), indicating no self-association or nonideality under these conditions. CaM binding causes a slight increase in the sedimentation constant consistent with the mass increase. Moreover, there is no evidence of dimer or oligomer formation. Also, no evidence of dimerization was found for the 77k-MLCK or 61k-MLCK fragments (Figure 7).

The sedimentation velocity results indicate that recombinant rabbit smooth muscle MLCK is a highly asymmetric molecule with an observed mass of 126 kg/mol, a sedimentation coefficient ($s_{20,w}$) of 3.94, and a frictional coefficient due to shape alone (f/f_o) of 1.92 (Table 1). If modeled as a prolate ellipsoid of revolution using the Perrin equation, the molecule would have an a/b axial ratio of 18.0 and a hydrodynamic length and a hydrodynamic width of 53.4 and 3.0 nm, respectively (Table 1). This is consistent with the results of Ausio et al. (*29*), who found the slightly smaller turkey gizzard MLCK (M = 108 kg/mol) also to be highly asymmetric ($s_{20,w}$ = 3.74, f/f_o = 1.95, and a/b = 18.9). Also asymmetric is MLCK isolated from rabbit skeletal muscle (*2*, *28*). Much of the asymmetry of smMLCK must be attributable to the N-terminal part of the molecule since 77k-MLCK and 61k-MLCK have axial ratios of 8.8 and 7.7, respectively, and corresponding hydrodynamic lengths of 28 and 24 nm, respectively (Table 1). CaM binding causes a slight decrease in the axial ratios, which can be attributed to an increase in the apparent widths. This is consistent with CaM binding to the catalytic domain of MLCK causing some structural rearrangement (*57*).

Structural Homology Modeling of smMLCK. Implicit in the calculation of the molecular dimensions of smMLCK from the sedimentation velocity data (Table 1) is the assumption that the shape of the molecule can be approximated by a regular geometrical shape such as a prolate ellipsoid. This approximation may yield a reasonable representation of globular proteins and those proteins that have a uniform distribution of mass. Judging from the EM images in Figure 3, this is clearly not the case for smMLCK. There is a clear difference between the highly structured C-terminal and flexible N-terminal parts of the molecule. Thus, the dimensions of smMLCK calculated from sedimentation velocity data may not represent its molecular shape in solution. To obtain a more realistic representation of the mass distribution in smMLCK, we have used the structural homology modeling approach. As described in the introductory section, smMLCK has a modular structure similar in many respects to the megadalton muscle protein titin. Extensive studies on titin have shown that the individual immunoglobulin-related (Ig) and fibronectin-related (Fn) domains are folded independently and the molecule can be represented as a linear arrangement of the individual domains (*58*, *59*). We have modeled the domains of smMLCK and tested how their relative arrangement would affect the predicted sedimentation coefficients as calculated with HYDROPRO (*50*). As the EM images indicate, it is highly unlikely that there is a unique or even a predominant structure of smMLCK in solution. Thus, it would be futile to attempt to obtain a precise atomic structure of the entire molecule. Our goal was to combine the available biochemical,

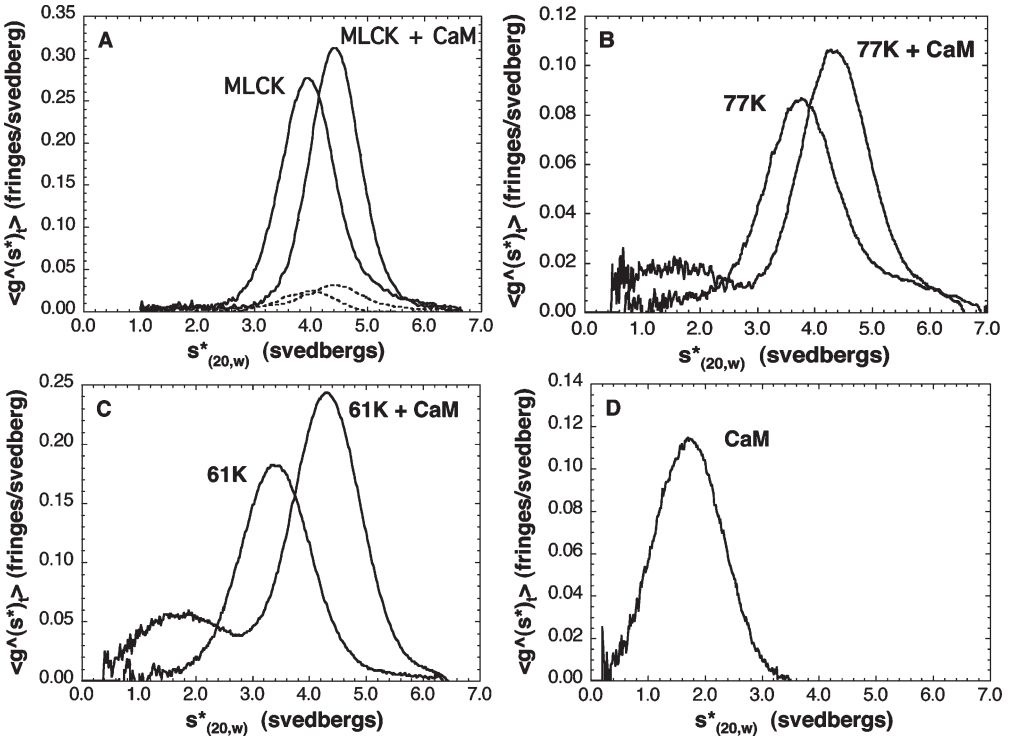

FIGURE 7: Sedimentation velocity profiles of smMLCK and its fragments in the absence and presence of CaM: (A) full-length smMLCK at 0.13 mg/mL (—) and at a 10-fold dilution (---), (B) 77k-MLCK, (C) 61k-MLCK, and (D) calmodulin. The protein samples (0.13−0.2 mg/mL) were dialyzed against a solution containing 0.1 M NaCl, 1 mM $MgCl_2$, 20 mM MOPS (pH 7.0), and 1 mM $CaCl_2$.

Table 1: Hydrodynamic Parameters of the Recombinant Rabbit Smooth Muscle MLCK and Its 61k and 77k C-Terminal Fragments Alone and in Complexes with CaM

	MLCK	MLCK−CaM	77k	77k−CaM	61k	61k−CaM	CaM
no. of amino acids	1147	1295	687	835	542	690	148
hydration δ_1	0.433	0.436	0.428	0.434	0.410	0.421	0.460
specific volume v_2	0.737	0.735	0.731	0.730	0.735	0.732	0.723
calculated mass (kDa)	125.7	142.4	77.3	94.0	61.2	77.9	16.7
observed mass (kg/mol)	126	142	77.3	90.8	63.2	79.7	17.1
sedimentation coefficient $s_{20,w}$	3.94	4.42	3.78	4.32	3.42	4.30	1.72
frictional ratio f/f_o	1.92	1.86	1.48	1.44	1.41	1.32	1.20
axial ratio a/b	18.0	16.8	8.8	8.2	7.7	6.2	4.2
length (Å)	530	530	280	280	240	220	100
width (Å)	30	32	32	34	31	36	25
stokes radius R_s (Å)	74.3	75.2	48.5	50.4	43.4	44.1	23.8

physicochemical, and structural information to improve our understanding of smMLCK function. Below is a description of our approach, and the summary, including the definition of the domains and the list of structural templates used for their modeling, is given in Table 2.

C-Terminal Region of smMLCK. (*i*) *Kinase/Regulatory Domain*. The catalytic domain of smMLCK can be modeled with a high degree of confidence because the domain has a high degree of sequence similarity with other kinases and undoubtedly follows their common structural framework (*3*). Knighton at al. have modeled the catalytic core of smooth muscle MLCK (*60*) using the crystallographic coordinates of the cyclic AMP-dependent protein kinase catalytic subunit and a bound pseudosubstrate inhibitor peptide (*61*, *62*). They have shown that despite only 30% identity of the amino acid sequence, smMLCK can be readily accommodated in that structure. Their model contains 262 amino acids corresponding to residues 689−951 of rabbit smMLCK and includes the catalytic core and the pseudosubstrate inhibitory segment. A more inclusive template for modeling smMLCK that we used here is the structure of twitchin kinase [Protein Data Bank (PDB) entry 1koa (*63*)]. Twitchin is a 753 kDa protein (6839 residues) located in the muscle A-band of the nematode *Caenorhabditis elegans*. The structure of twitchin kinase contains the catalytic core and a 60-residue C-terminal autoinhibitory region that extends through the active site and provides direct intrasteric inhibition of kinase activity analogous to that of smMLCK (*63*). The twichin kinase structure also contains at the C-terminus an Ig domain similar to the telokin region of smMLCK. Modeling of the smMLCK kinase domain required insertion of two loops that were missing in twitchin. Also, in the structure of twitchin kinase, there is an N-terminal extension that is not present in the other kinase structures. This segment has a low degree of sequence similarity to the corresponding region of smMLCK; however, its inclusion in the model enabled us to position the N-terminally adjacent Ig2−Fn3 tandem on the opposite side of

Table 2: Definition of the Structural Domains and Segments of Rabbit Smooth Muscle MLCK Used in Model Building[a]

domain name	residue range	no. of amino acids	mass (kDa)	template	ref
actin-binding domain	1−99	99	10.668	extended	
16 × 12 tandem repeat (PEVK)	*100−294*	*195*	*19.881*	*poly-Pro type II helix*	
linker 1	*295−327*	*33*	*3.581*	*extended*	
Ig1	**328−419**	**92**	**10.016**	**2yr3**	*82*
linker 2	*420−464*	*45*	*4.739*	*extended*	
Ig2−Fn3 tandem	**465−657**	**193**	**21.397**	**2nzi**	*65*
linker 3	658−689	32	3.750	extended/1koa	
kinase/regulatory domain	**690−1002**	**313**	**35.712**	**1koa, 1kob, 1tki**	*83* and *84*
linker 4	1003−1038	36	3.871	1koa	
Ig3 (telokin)	**1039−1134**	**96**	**10.807**	**1tlk, 1koa**	*26* and *83*
poly-Glu	*1135−1147*	*13*	*1.479*	*extended*	

[a]Bold type denotes residues modeled with a high degree of confidence [694 amino acids total (62.0% of the mass)]. Italics denote predicted flexible regions [286 amino acids total (23.6% of the mass)]. The 167 remaining residues, which include the actin-binding domain, linker 3, and linker 4, are likely to have well-defined structures and to make little contribution to MLCK flexibility. Note that 61k-MLCK, which comprises the Ig2−Fn3 tandem, linker 3, and the kinase domain (residues 461−1002), is equivalent to the trypsin resistant fragment of smMLCK. The following templates were used for modeling: for Ig1, 2yr3, the solution structure of the fourth Ig-like domain from myosin light chain kinase (*82*); for the Ig2−Fn3 tandem, 2nzi, Ig(A169)−FnIII(A170) segment directly preceding the kinase domain of titin (*65*); for the kinase domain, 1kob, the kinase domains of twitchin from *Aplysia*, 1koa, the kinase and telokin region of twitchin from *Caenorhabditis elegans* (*83*), and 1tki, the kinase domain of titin (*84*); for Ig3, 1tlk, telokin from turkey gizzard (*26*).

the telokin domain, thus facilitating the linear arrangement of the domains.

(*ii*) *Immunoglobulin- and Fibronectin-Related Motifs.* As mentioned in the introductory section, the structure of the C-terminal Ig3 region (telokin) from turkey gizzard MLCK is the only part of smMLCK whose high-resolution structure is known (*26*). The structure is a typical β-sandwich Ig fold containing seven β-strands (*64*). In view of the amino acid sequence similarity of the Ig3 domain of rabbit smMLCK and turkey gizzard MLCK, it was straightforward to model residues 1039−1136 of rabbit smMLCK using telokin as a template (PDB entry 1tlk). However, there is uncertainty concerning the N-terminal part of telokin, which in the full-length MLCK makes a connection to the kinase/regulatory domain. The telokin structure begins at residue 33 (residue 1032 of smMLCK) with a stretch of six amino acids in an extended conformation that does not belong to the Ig fold. These residues were not considered in our modeling, and the position of the Ig3 domain with respect to the kinase domain was modeled on the basis of the twitchin kinase structure (*63*) (PDB entry 1koa).

The Fn3 module comprises on average 90 residues and has a typical double-β-sheet sandwich structure in which the two sheets have a right-handed twist and pack against each other face to face. The structure of this motif is similar to the Ig modules differing mainly in a switch of a single β-strand between the sheets (*64*). Structures of the two remaining Ig domains of smMLCK could be modeled with a high degree of confidence despite a relatively low degree of amino acid sequence identity with the templates. The modeling was straightforward due to the fact that there are many high-resolution Ig-type structures in the PDB and the rules relating the amino acid sequence to the 3D structure of this common protein fold are well-known. The relative disposition of the Ig2 and Fn3 regions of smMLCK was modeled on the basis of the structure of one of the Ig2−Fn3 tandem repeats of titin (*65*) (PDB entry 2nzi) (Figure 1).

(*iii*) *Models of 61k-MLCK and 77k-MLCK.* 61k-MLCK comprises the Ig2−Fn3 tandem, the catalytic/regulatory domain, and a short linker connecting the two structures (Table 2). The linker defines the distance and the relative orientation of the Ig2−Fn3 tandem with respect to the catalytic domain. We have constructed three models of 61k-MLCK. In model 1, the long

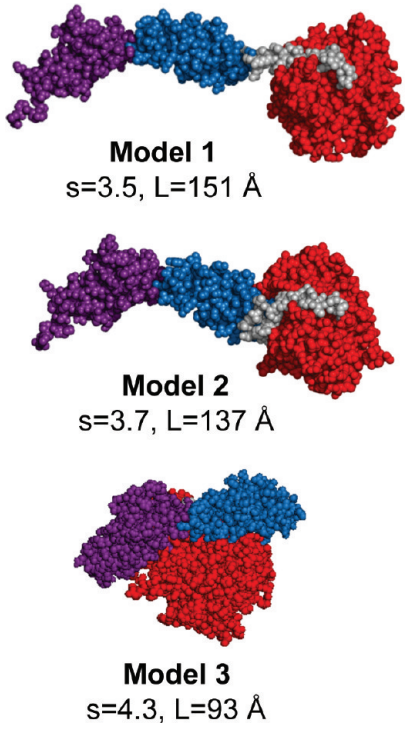

FIGURE 8: Models of the 61k fragment of smMLCK. Three different arrangements of the Ig2−Fn3 tandem with respect to the catalytic domain were tested. The domains are color-coded: red for the catalytic/regulatory domain, blue for the Fn3 domain, magenta for the Ig(2) domain, and gray for the linker region (linker 3) connecting the Fn3 domain with the catalytic domain. See Table 2 for the exact definition of the domains. Images of protein models were generated with PyMOL (*85*).

axis of the Ig2−Fn3 tandem points toward the kinase domain. The linker is structured as a helical segment projecting away from the catalytic domain, which precludes any contacts between the Ig2−Fn3 tandem and the kinase domain (Figure 8). In model 2, the orientation of the Ig2−Fn3 tandem is similar to that in model 1, but the linker region is collapsed, allowing tight contacts between the Ig2−Fn3 tandem and the kinase domain. This arrangement causes the overall length of the molecule to decrease by 14 Å (9.3%). In model 3, the Ig2−Fn3 tandem is flipped back and tightly packed against the kinase domain to simulate the

hypothetical compact conformation suggested by the EM. The corresponding models of 77k-MLCK were constructed via addition of the Ig3 domain at the C-terminus of each of the three models of 61k-MLCK. The orientation of the Ig3 domain with respect to the kinase domain was similar to that in the twitchin kinase. For all the models, the theoretical sedimentation coefficients were calculated with HYDROPRO (*50*) (see below).

N-Terminal Region and Linker Segments of smMLCK. In contrast to the well-structured C-terminal part of smMLCK, we found no templates suitable for modeling the N-terminal 327-amino acid segment of this protein. This includes the actin-binding domain, the 16 × 12 tandem repeat (PEVK), and the 30-residue linker connecting the PEVK region to the first Ig domain (see Table 2). The secondary structure prediction yielded "coil" assignment to the entire region. To assess the contribution of this poorly structured segment to the hydrodynamic properties of smMLCK, we used the following approach.

(*i*) *Actin-Binding Domain*. Although there are many proteins that bind F-actin, the actin-binding domain of smMLCK (residues 1−99) appears to have a unique amino acid sequence and a unique binding site on F-actin. Hatch et al. (*16*) were able to see the density of this fragment bound to F-actin in the 3D reconstructions of EM images, suggesting that this part of smMLCK has a defined structure in the presence of the target. However, it must be an extended structure, since this segment interacts apparently with three actin monomers (*15*); i.e., it has to span ~150 Å. Thus, it is likely that in solution in the absence of F-actin this region is unstructured and may be represented as random coil. Accordingly, we have initially modeled the 99 N-terminal residues of smMLCK in the extended conformation and subjected it to 100 ps of molecular dynamics in vacuo, which caused it to collapse into a relatively compact random structure. There is no significance in such a representation other than the convenience of subsequent positioning of the corresponding mass in a model of smMLCK a defined distance from the C-terminal structured domains. Such a representation is akin to the common practice in hydrodynamic modeling of representing various parts of a protein in the form of appropriately sized beads.

(*ii*) *The 16 × 12 Tandem Repeat* (*PEVK*). On the C-terminal side of the actin-binding region of rabbit smMLCK is a 16-fold repeat of a 12-residue segment, TLKPV(G,A)N-(A,I,T)KPAE (*10*). This segment has been termed the PEVK region, the name coined for the segments rich in Pro, Glu, Val, and Lys found in the megadalton muscle protein titin. An essential difference between the repetitive segment of mammalian smMLCK and the PEVK region of titin is that in the latter the sequence is less regular. An almost exact repetition of a 12-residue motif in MLCK suggests some regular structural features. Searching the Gene Bank with BLAST, we found sequence similarity to several prokaryotic and eukaryotic proteins, including neurofilament triplet H protein, neural cell adhesion molecule, T-cell adhesion receptor CD2 domain, chicken prion protein, etc. The sequence similarity is restricted, however, to the six-residue spacing of the Pro and/or Lys residues. It has been suggested that similar Pro-rich repetitive sequences in the bacterial cell wall have a poly-Pro type II helix conformation (*66*). There is also evidence that the poly-Pro type II helix is the predominant structure in the PEVK region of titin and that the dynamic properties of this structure make a major contribution to titin's elasticity and extensibility (*17*, *67*−*69*). The far-UV CD spectrum of a synthetic peptide spanning two 12-residue repeats of smMLCK shows a strong negative peak at 198 nm (Figure 9). Similar CD spectra have been attributed to the poly-Pro type II helix (*66*, *67*, *70*, *71*). Thus, we have modeled the 16 × 12 tandem repeat region of smMLCK as a polyproline type II helix (ϕ = −75°, ψ = 145°, and ω = 180°). In this conformation, there are exactly three residues per turn and the carbonyl oxygen atoms of the peptide bonds point away from the helix axis, allowing stabilization by hydrogen bonding with water. In this conformation, the 195 amino acids of the 16 × 12 tandem repeat span 590 Å (3.0 Å/residue). The initial model has been subjected to molecular dynamics simulations for various times from 50 to 300 ps, which resulted in a partial collapse of the structure. Interestingly, even though no further compaction was observed after MD for 300 ps, as judged by a nearly constant count of interatomic contacts, the structure was not fully randomized and retained some regular features. Most notably, all $i-i \pm 3$ electrostatic side chain interactions between Glu and the flanking Lys residues were retained (Figure 9C). The partially collapsed structures of the 16 × 12 tandem repeat region were used to construct the three models of full-length smMLCK shown in Figure 10.

(*iii*) *Linker Regions*. In addition to the regions of smMLCK discussed above, there are short linker segments that cumulatively account for ~8% of the polypeptide chain. Their structure determines the relative position of the individual domains with respect to each other but unfortunately cannot be modeled with confidence. On the other hand, the variability of the shape and thus of domain arrangement in the EM images strongly suggests that these linkers are flexible and may be reasonably approximated by a random coil. We have generated models of the corresponding segments in the extended conformation (3.3 Å/residue in length) and subjected them to molecular dynamics simulation. This caused the polypeptide chain to collapse into a random and relatively compact conformation. The structure was considered to be in equilibrium if no further increase in the number of intramolecular interactions was observed during the molecular dynamics simulation. Typically, a 50−100 ps simulation was sufficient for the chain to reach equilibrium. These structures were joined with the other modeled segments and subjected to energy minimization to obtain the final models.

Validation of the Models. As a method of validation of the modeled structures, we have compared the theoretical sedimentation coefficients calculated from the atomic coordinates with those observed experimentally. We have used the hydrodynamic simulation procedure developed by Garcia de la Torre and colleagues (*50*, *72*) as implemented in HYDROPRO. In this procedure, a primary hydrodynamic model is built from atomic coordinates via replacement of non-hydrogen atoms with spherical elements of some fixed radius. The resulting particle consisting of overlapping spheres is, in turn, represented by a shell model, for which a number of hydrodynamic parameters, including the sedimentation coefficient, are calculated. The key adjustable parameter in these calculations is the so-called atomic element radius (AER), which provides the means of volume correction for hydration by artificially inflating the surface atoms. On the basis of the analysis of a number of reference proteins for which the hydrodynamic parameters and the high-resolution structures were known, Garcia de la Torre et al. concluded that an AER of 3.1 Å yields results that are most consistent with the experiment. In view of the fact that neither the hydration nor the 3D structures of our models were certain, we tested a range of AER values for each model and used calmodulin as a control. In Figure 11, the dependence of the theoretical

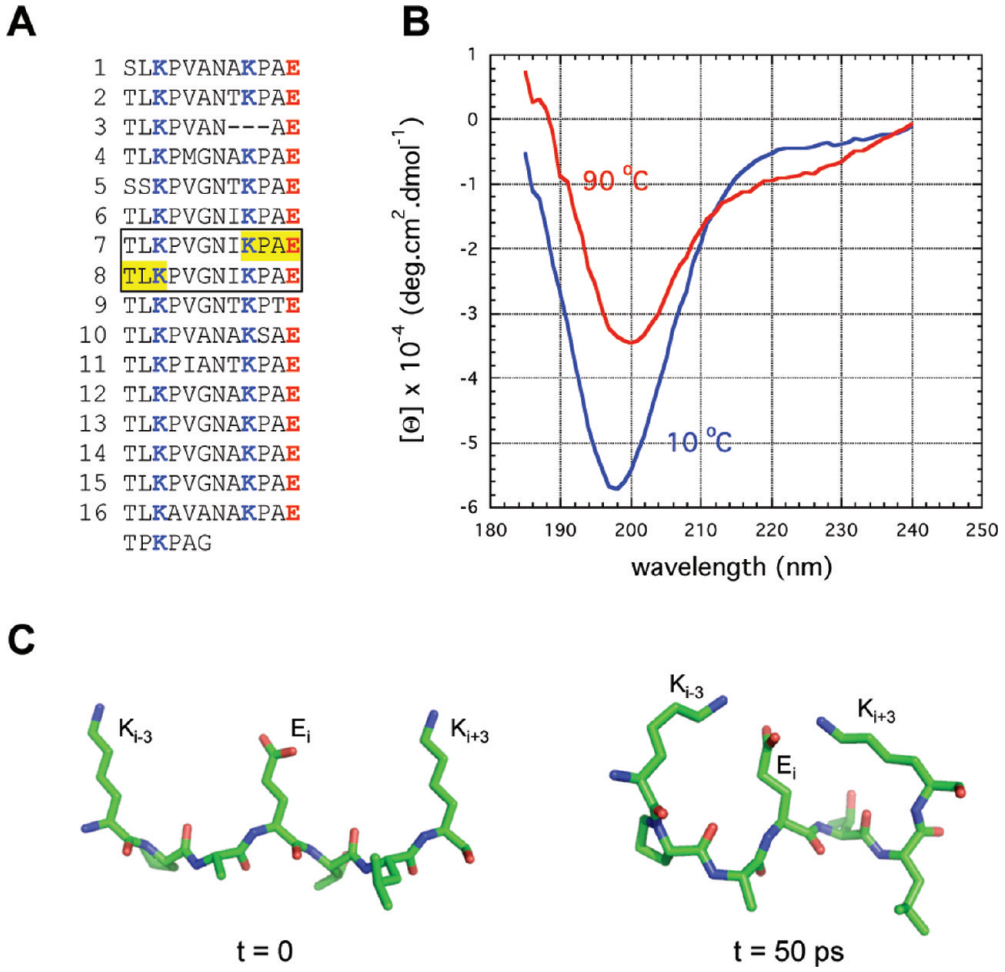

FIGURE 9: Structural features of the PEVK region of smMLCK. (A) Amino acid sequence showing the highly conserved repetitive nature of this segment. Note that each Glu residue is flanked on both sides with positively charged Lys side chains, which allow for the $i-i\pm3$ salt bridges in the poly-Pro helical configuration. (B) Far-UV circular dichroism spectra of a synthetic 24-residue peptide corresponding to the two 12-residue repeats marked by the rectangle in panel A. The negative peak at 198 nm is characteristic of poly-Pro helix type II. (C) Example of the Lys−Glu−Lys salt bridges in the modeled structure of the PEVK region of smMLCK. The initial configuration ($t = 0$) and the configuration after molecular dynamics simulation for 50 ps are shown.

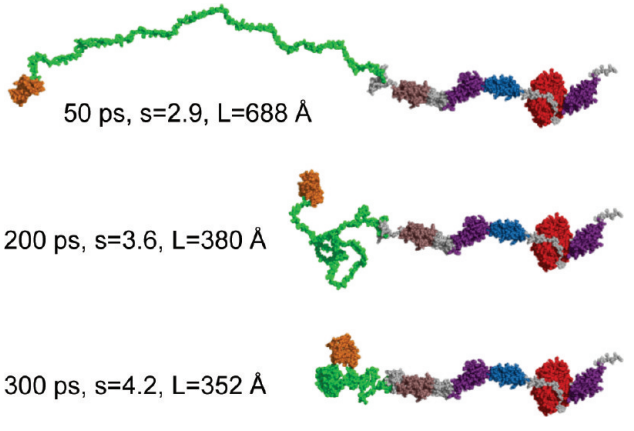

FIGURE 10: Modeling of the full-length smMLCK. The C-terminal part of the molecule starting at residue 327 modeled in the extended configuration corresponding to model 1 in Figure 8 is identical in all three models. The PEVK region (green) is subjected to MD simulation for 50, 200, and 300 ps, resulting in a progressive compaction of the polypeptide chain. The domains comprising 61k-MLCK are colored in the same manner as in Figure 8. All linker regions are colored gray; the N-terminal actin-binding domain is colored orange, the Ig1 domain brown, and the C-terminal telokin region (Ig3) magenta.

sedimentation coefficients on the AER for each of the structures is shown. For CaM, the AER values in the range of 2.5−3.0 Å provide a good agreement with the experiment. For 61k-MLCK and 77k-MLCK, only the most extended structures (cf. model 1 in Figure 8) yield the calculated sedimentation coefficients that are consistent with the experimental values. Most remarkably, the data in Figure 11 clearly show that model 2 of 61k-MLCK, which due to the more compact conformation of linker 3 is 14 Å (9.3%) shorter than model 1, cannot be correct, since the computed sedimentation coefficients are larger than the experimental value [$s_{20,w} = 3.4$ (cf. Table 1)] at any reasonable level of hydration. This example illustrates the sensitivity and the discriminative power of this approach. Interestingly, model 1 of 61k-MLCK is 151 Å long (Figure 8), which is significantly shorter (37%) than the long axis of the corresponding prolate ellipsoid calculated from the sedimentation data [240 Å (Table 1)]. Similarly, the length of the best model of 77k-MLCK is only 180 Å, and that of CaM is 74 Å, as opposed to 280 and 100 Å, respectively, for the corresponding prolate ellipsoids (Table 1). Thus, it is clear that the models of 61k-MLCK and 77k-MLCK obtained by structural homology modeling supported by the computation of the hydrodynamic parameters with HYDRO-PRO provide a much better estimate of the molecular shape and

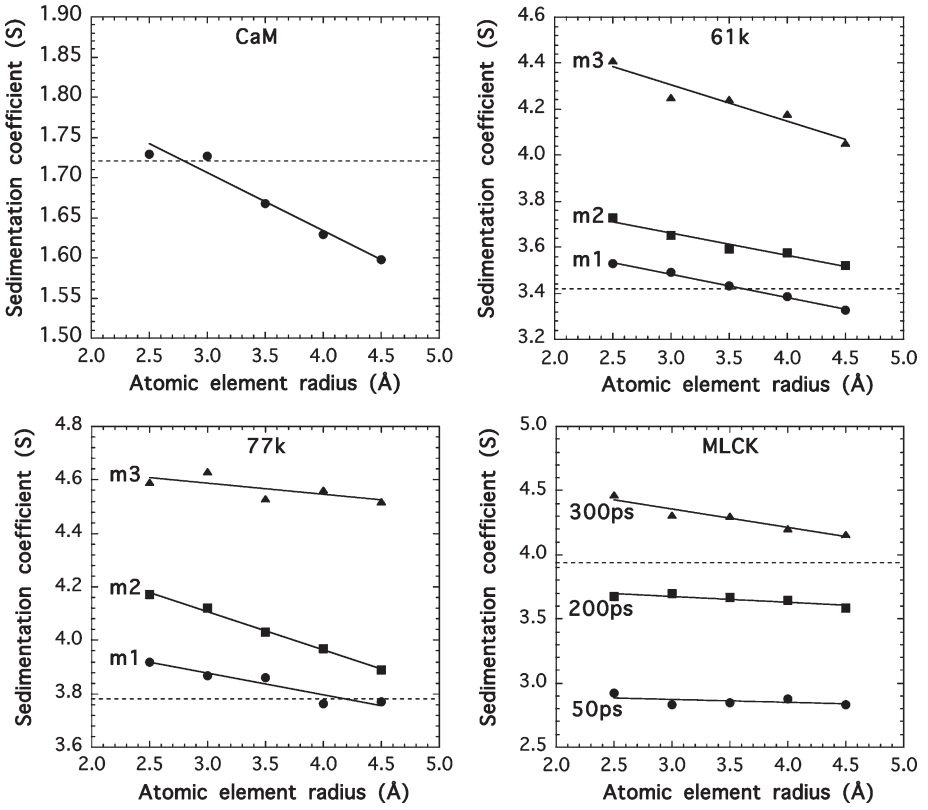

FIGURE 11: Sedimentation coefficients of CaM and MLCK models computed from their atomic coordinates. HYDROPRO was used for the calculations. The effect of hydration on the calculated sedimentation coefficients is tested by varying the so-called atomic element radius (AER). The dashed line in each panel shows the experimentally determined value of $s_{20,w}$ for each molecule. The abbreviations m1, m2, and m3 correspond to the three models of 61k-MLCK shown in Figure 8 and the respective models of 77k-MLCK as described in the text. Note that only the most extended models of the 61k- and 77k-MLCK fragments are consistent with the observed sedimentation coefficients. For the full-length MLCK, an extended C-terminal part combined with a moderately compacted PEVK region yields the *s* values consistent with the experiment.

dimensions of these molecules in solution than the commonly used prolate ellipsoid approximation.

On the basis of the data in Figure 11, we can conclude with reasonable confidence that the structural domains of the C-terminal part of smMLCK (residues 465−1147) are arranged in a linear fashion; i.e., the Ig2−Fn3 tandem is positioned on the opposite side of the catalytic/regulatory domain with respect to the telokin (Ig3) region. The long axis of the Ig2−Fn3 tandem is oriented in line with the long axis of the molecule, and the connecting region (linker 3, residues 658−689) has a semiextended conformation. The linker 3 region appears to be the main, if not the only, source of flexibility in 61k-MLCK. We used the most extended model of 77k-MLC (model 1) to construct three models of the full-length smMLCK differing in the extent of compaction of the PEVK region (Figure 10). Although for none of the models could the computed sedimentation coefficient match precisely the experimental data at any level of hydration, the model having a moderately compacted PEVK region provided the best approximation. Thus, our estimate of the length of smMLCK in solution is 350−380 Å. This is significantly shorter than the value of 530 Å calculated for the long axis of the corresponding prolate ellipsoid (Table 1), but both estimates are well within the broad range of the contour length distribution of smMLCK cross-linked to F-actin (Figures 3 and 4). The C-terminal 77k segment contributes approximately one-half (180 Å) to the total length of smMLCK in solution. The actin-binding domain, the PEVK region, and linker 1 account for the remaining ~180 Å. As pointed out earlier and experimentally documented for the PEVK region of titin, the poly-Pro type II helix is highly flexible and extensible. If stretched, the PEVK region of smMLCK could contribute up to 590 Å to the length of smMLCK (in the poly-Pro helix type II conformation) or even as much as 640 Å in the fully extended conformation. Thus, our results indicate that the smMLCK molecule is not only elongated, as previously reported for turkey gizzard (*29*), but also exceptionally flexible and extensible.

DISCUSSION

We have applied structural homology, molecular dynamics, and hydrodynamic modeling methods to obtain an approximate all-atom representation of smMLCK, a 125 kDa multidomain protein. We have tested different spatial arrangements of the Ig and Fn3 domains with respect to the catalytic domain of smMLCK and demonstrated that to account for the experimentally determined sedimentation coefficients these domains must be arranged in a linear fashion with respect to the long axis of the molecule. The model of smMLCK that emerges from this work is of a highly elongated molecule with a nonuniform mass distribution. It has a well-structured C-terminal part in which the catalytic domain is located and a poorly structured, extensible segment in the N-terminal part. Such a model is consistent with our EM images of smMLCK cross-linked to F-actin and sedimentation velocity measurements on the full-length smMLCK and its two catalytically active C-terminal fragments.

The average length of smMLCK in solution obtained by the modeling approach is 350−380 Å, which is significantly shorter (~30%) than the length calculated from the sedimentation velocity data using the Perrin equation for a prolate ellipsoid

[530 Å (cf. Table 1)]. A question of which approach provides a better estimate of the molecular dimensions of smMLCK in solution arises. Our sedimentation velocity data for the mammalian smMLCK (1147 amino acids) are consistent with those obtained by Ausio et al. (*29*) for the slightly smaller (972 amino acids) turkey gizzard MLCK. They have reported a sedimentation coefficient $s_{20,w}$ of 3.74, a Stokes radius R_s of 68.5 Å, and a length L of 499 Å, which compare favorably to our results for smMLCK: $s_{20,w} = 3.94$, $R_s = 74.3$ Å, and $L = 530$ Å (Table 1). Thus, we are confident that our recombinant smMLCK is folded properly and our measurements are correct. Still, in our view, the HYDROPRO modeling approach provides a better estimate of the molecular dimensions of smMLCK despite the uncertainties in modeling the flexible segments and the arbitrary assumptions with respect to the relative spatial positioning of the domains. The key advantage of the modeling approach is that it takes into account the highly nonuniform mass distribution in MLCK. In contrast, the prolate ellipsoid approximation used for the calculation of molecular dimensions from the sedimentation velocity data assumes idealized uniform mass distribution, which is clearly incorrect for MLCK. Interestingly, the prolate ellipsoid approximation overestimates the length by ~25% for our "control" protein calmodulin, which is less asymmetric than smMLCK, as revealed by the high-resolution X-ray and NMR structures. On the basis of these considerations, we conclude that the average length of smMLCK in solution is in the range of 350−380 Å. However, it is not clear if this estimate is applicable to the conditions in smooth muscle, where the constraints of the cellular environment might restrict the conformational dynamics of smMLCK, causing it to assume a more compact structure. Conversely, because of the location of the actin and myosin binding sites at the extreme N- and C-termini of the molecule, respectively, smMLCK might bridge the F-actin and myosin filaments (see below) and under certain conditions undergo significant stretching. Under stretch, the poorly structured repetitive segment alone could span >600 Å, which would enable the catalytic domain of smMLCK to extend up to 750 Å from the F-actin filament to which it is bound by its N-terminus.

Our model of smMLCK enables us to consider from a structural perspective the properties of this protein well-known from other studies and to make inferences with respect to its function in the activation of smooth muscle contraction. The key properties to be considered are (1) the elongated, flexible, and extensible shape, (2) the catalytic/regulatory domain that is located at the opposite end of the polypeptide chain from the actin-binding site, and (3) a noncatalytic myosin-binding site at the extreme C-terminus of the molecule. These properties combined with the observation that smMLCK is virtually immobilized in smooth muscle cells (*30*) suggest a functional model in which, in addition to its catalytic function, smMLCK provides a structural link between the thin and thick filaments (Figure 12). In this model, smMLCK is pictured as a flexible, extensible molecule bound to the actin filaments, but capable of extending to and activating the myosin heads at a significant distance without detaching from F-actin. Such a function is clearly possible in view of the fact that the estimated distance between the thin and thick filaments in smooth muscle is only ~150 Å (*73*), which is less than half of the average length of smMLCK in solution estimated in this work. Furthermore, the extensibility of the PEVK region enables the catalytic domain to extend even farther from the actin filament which is evident from the data in Figures 3 and 4, and from the structural arguments discussed above. In their 1998 review article, Stull et al. (*27*) considered the possibility that the fully extended MLCK could span ~600 Å and bridge the thick and thin filaments in smooth muscle. However, no experimental evidence of the linear domain arrangement was presented, nor were alternative models considered. If indeed smMLCK bridges thin and thick filaments, a question of whether this could inhibit filament sliding during contraction arises. It has been shown that MLCK binding to phosphorylated myosin is much weaker than that to unphosphorylated myosin heads. Thus, alternating between strong and weak binding of smMLCK to myosin might be sufficient to allow for filament sliding and muscle contraction.

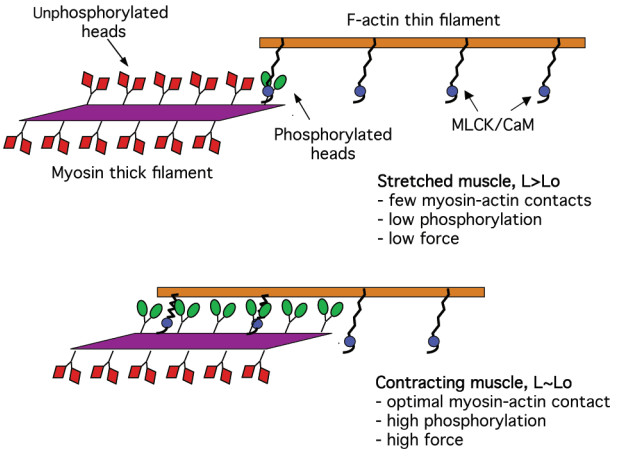

FIGURE 12: Hypothetical mechanism of myosin phosphorylation in mammalian smooth muscle. smMLCK is pictured as a flexible, extensible molecule bound to actin filaments and capable of bridging thin and thick filaments. Those myosin heads that are in contact with actin filaments are phosphorylated preferentially and thus become capable of producing force. The number of activated myosin heads depends on filament overlap. Dissociation of the catalytic domain of smMLCK from phosphorylated myosin heads enables filament sliding. smMLCK might contribute to the passive tension under resting conditions by bridging the thick and thin filaments.

The binding of smMLCK to F-actin is well-documented (*11*, *12*); the interaction sites are identified (*13*, *15*, *74*, *75*), and even the low-resolution structure is determined (*16*). However, the question of whether in smooth muscle cells smMLCK is primarily associated with F-actin or with myosin filaments is still a controversial issue. The equilibrium dissociation constant for smMLCK binding to myosin in vitro is in the micromolar range (*12*); however, there is also a fraction of MLCK that binds very tightly with nanomolar affinity and copurifies with myosin (*76*−*78*), suggesting the possibility of subpopulations of smMLCK. Recently, Cremo and her colleagues (*79*) explored the properties of purified smooth muscle myosin preparations that contained tightly bound MLCK. They have shown that such myosin is capable of supporting F-actin motility in vitro in a Ca^{2+}-dependent manner without additional MLCK and calmodulin. Thus, the small amounts of MLCK associated with myosin (by their estimate a MLCK:myosin ratio as low as 1:73) were sufficient to phosphorylate myosin and to support F-actin motility. Interestingly, the maximum F-actin velocity was approximately one-half of the velocity with pre-thiophosphorylated myosin (*79*). These observations suggest that each molecule of smMLCK is capable of acting on many myosin heads despite the strong binding, or perhaps because of an unknown mechanism that enables sequential phosphorylation (e.g., that presented in Figure 12).

An interesting feature of the hypothetical mechanism shown in Figure 12 is that it might provide efficient means for the preferential activation of myosin heads that are in direct contact with F-actin filaments and thus upon phosphorylation can be immediately involved in force generation. This might facilitate efficient energy utilization in smooth muscle, since no ATP would be used for phosphorylation of myosin heads that are far from the actin filaments, e.g., under stretch. Our model predicts that the number of activated myosin heads, i.e., the level of phosphorylation, should be proportional to the filament overlap. Such an effect was observed in permeabilized rabbit femoral artery smooth muscle strips (T. Kitazawa, personal communication). The fraction of phosphorylated LC20 changed with cell length in a manner similar to that of the force, being the highest at L_o (43.7% LC20 phosphorylation) and significantly lower in the contracted (13.8%) and stretched (6.5%) muscles. More experiments are needed to verify this finding and demonstrate its generality.

The potential contribution of smMLCK to the structure of smooth muscle requires a comment. It has been proposed that titin, the protein structurally related to smMLCK, is the major contributor to passive tension in striated muscles. Recent studies also suggest that titin plays an important role in the length-dependent activation by sensing stretch and promoting actomyosin interaction (*80*, *81*). There is clearly a significant similarity between the properties of titin and smMLCK. In particular, because of the elasticity of the PEVK region, smMLCK molecules might affect the interfilament spacing and contribute to the passive tension in smooth muscle.

REFERENCES

1. Walsh, M. P., Dabrowska, R., Hinkins, S., and Hartshorne, D. J. (1982) Calcium-independent myosin light chain kinase of smooth muscle. Preparation by limited chymotryptic digestion of the calcium ion dependent enzyme, purification, and characterization. *Biochemistry 21*, 1919–1925.
2. Mayr, G. W., and Heilmeyer, L. M., Jr. (1983) Skeletal muscle myosin light chain kinase. A refined structural model. *FEBS Lett. 157*, 225–231.
3. Taylor, S. S., Knighton, D. R., Zheng, J., Ten Eyck, L. F., and Sowadski, J. M. (1992) Structural framework for the protein kinase family. *Annu. Rev. Cell Biol. 8*, 429–462.
4. Pearson, R. B., Wettenhall, R. E., Means, A. R., Hartshorne, D. J., and Kemp, B. E. (1988) Autoregulation of enzymes by pseudosubstrate prototopes: Myosin light chain kinase. *Science 241*, 970–973.
5. Kemp, B. E., Pearson, R. B., House, C., Robinson, P. J., and Means, A. R. (1989) Regulation of protein kinases by pseudosubstrate prototopes. *Cell. Signalling 1*, 303–311.
6. Gallagher, P. J., Herring, B. P., Trafny, A., Sowadski, J., and Stull, J. T. (1993) A molecular mechanism for autoinhibition of myosin light chain kinases. *J. Biol. Chem. 268*, 26578–26582.
7. Gallagher, P. J., Herring, B. P., and Stull, J. T. (1997) Myosin light chain kinases. *J. Muscle Res. Cell Motil. 18*, 1–16.
8. Herring, B. P., Stull, J. T., and Gallagher, P. J. (1990) Domain characterization of rabbit skeletal muscle myosin light chain kinase. *J. Biol. Chem. 265*, 1724–1730.
9. Olson, N. J., Pearson, R. B., Needleman, D. S., Hurwitz, M. Y., Kemp, B. E., and Means, A. R. (1990) Regulatory and structural motifs of chicken gizzard myosin light chain kinase. *Proc. Natl. Acad. Sci. U.S.A. 87*, 2284–2288.
10. Gallagher, P. J., Herring, B. P., Griffin, S. A., and Stull, J. T. (1991) Molecular characterization of a mammalian smooth muscle myosin light chain kinase. *J. Biol. Chem. 266*, 23936–23944 [erratum, (1992) *J. Biol. Chem. 267*, 9450].
11. Dabrowska, R., Hinkins, S., Walsh, M. P., and Hartshorne, D. J. (1982) The binding of smooth muscle myosin light chain kinase to actin. *Biochem. Biophys. Res. Commun. 107*, 1524–1531.
12. Sellers, J. R., and Pato, M. D. (1984) The binding of smooth muscle myosin light chain kinase and phosphatases to actin and myosin. *J. Biol. Chem. 259*, 7740–7746.
13. Kanoh, S., Ito, M., Niwa, E., Kawano, Y., and Hartshorne, D. J. (1993) Actin-binding peptide from smooth muscle myosin light chain kinase. *Biochemistry 32*, 8902–8907.
14. Lin, P. J., LubyPhelps, K., and Stull, J. T. (1997) Binding of Myosin Light Chain Kinase to Cellular Actin-Myosin Filaments. *J. Biol. Chem. 272*, 7412–7420.
15. Smith, L., Su, X., Lin, P., Zhi, G., and Stull, J. T. (1999) Identification of a novel actin binding motif in smooth muscle myosin light chain kinase. *J. Biol. Chem. 274*, 29433–29438.
16. Hatch, V., Zhi, G., Smith, L., Stull, J. T., Craig, R., and Lehman, W. (2001) Myosin light chain kinase binding to a unique site on F-actin revealed by three-dimensional image reconstruction. *J. Cell Biol. 154*, 611–617.
17. Tskhovrebova, L., Trinick, J., Sleep, J. A., and Simmons, R. M. (1997) Elasticity and unfolding of single molecules of the giant muscle protein titin. *Nature 387*, 308–312.
18. Witt, C. C., Olivieri, N., Centner, T., Kolmerer, B., Millevoi, S., Morell, J., Labeit, D., Labeit, S., Jockusch, H., and Pastore, A. (1998) A survey of the primary structure and the interspecies conservation of I-band titin's elastic elements in vertebrates. *J. Struct. Biol. 122*, 206–215.
19. Maruyama, K. (1997) Connectin/titin, giant elastic protein of muscle. *FASEB J. 11*, 341–345.
20. Ikebe, M., Stepinska, M., Kemp, B. E., Means, A. R., and Hartshorne, D. J. (1987) Proteolysis of smooth muscle myosin light chain kinase. Formation of inactive and calmodulin-independent fragments. *J. Biol. Chem. 262*, 13828–13834.
21. Ikebe, M., Maruta, S., and Reardon, S. (1989) Location of the inhibitory region of smooth muscle myosin light chain kinase. *J. Biol. Chem. 264*, 6967–6971.
22. Stull, J. T., Krueger, J. K., Kamm, K. E., Gao, Z.-H., Zhi, G., and Padre, R. (1996) Myosin light chain kinase. In Biochemistry of smooth muscle contraction (Barany, M., Ed.) pp 119−130, Academic Press, San Diego.
23. Ito, M., Dabrowska, R., Guerriero, R., and Hartshorne, D. J. (1989) Identification in turkey gizzard of an acidic protein related to the C-terminal portion of smooth muscle myosin light chain kinase. *J. Biol. Chem. 264*, 13971–13974.
24. Collinge, M., Matrisian, P. E., Zimmer, W. E., Shattuck, R. L., Lukas, T. J., Van, E. L., and Watterson, D. M. (1992) Structure and expression of a calcium-binding protein gene contained within a calmodulin-regulated protein kinase gene. *Mol. Cell. Biol. 12*, 2359–2371.
25. Silver, D. L., Vorotnikov, A. V., Watterson, D. M., Shirinsky, V. P., and Sellers, J. R. (1997) Sites of interaction between kinase-related protein and smooth muscle myosin. *J. Biol. Chem. 272*, 25353–25359.
26. Holden, H. M., Ito, M., Hartshorne, D. J., and Rayment, I. (1992) X-ray structure determination of telokin, the C-terminal domain of myosin light chain kinase, at 2.8 Å resolution. *J. Mol. Biol. 227*, 840–851.
27. Stull, J. T., Lin, P. J., Krueger, J. K., Trewhella, J., and Zhi, G. (1998) Myosin light chain kinase: Functional domains and structural motifs. *Acta Physiol. Scand. 164*, 471–482.
28. Mayr, G. W., and Heilmeyer, L. M. G. J. (1983) Shape and substructure of skeletal muscle myosin light chain kinase. *Biochemistry 22*, 4316–4326.
29. Ausio, J., Malencik, D. A., and Anderson, S. R. (1992) Analytical sedimentation studies of turkey gizzard myosin light chain kinase and telokin. *Biophys. J. 61*, 1656–1663.
30. Lin, P., Luby-Phelps, K., and Stull, J. T. (1999) Properties of filament-bound myosin light chain kinase. *J. Biol. Chem. 274*, 5987–5994.
31. Spudich, J. A., and Watt, S. (1971) The regulation of rabbit skeletal muscle contraction. I. Biochemical studies of the interaction of the tropomyosin-troponin complex with actin and the proteolytic fragments of myosin. *J. Biol. Chem. 246*, 4866–4871.
32. Tan, R. Y., Mabuchi, Y., and Grabarek, Z. (1996) Blocking the Ca^{2+}-induced conformational transitions in calmodulin with disulfide bonds. *J. Biol. Chem. 271*, 7479–7483.
33. Stafford, W. F. (1992) Boundary analysis in sedimentation transport experiments: A procedure for obtaining sedimentation coefficient distributions using the time derivative of the concentration profile. *Anal. Biochem. 203*, 295–301.
34. Stafford, W. F. (1994) Boundary analysis in sedimentation velocity experiments. *Methods Enzymol. 240*, 478–501.
35. Liu, S., and Stafford, W. F. (1995) An optical thermometer for direct measurement of cell temperature in the Beckman instruments XL-A analytical ultracentrifuge. *Anal. Biochem. 224*, 199–202.
36. Stafford, W. F., and Sherwood, P. J. (2004) Analysis of heterologous interacting systems by sedimentation velocity: Curve fitting

algorithms for estimation of sedimentation coefficients, equilibrium and kinetic constants. *Biophys. Chem. 108*, 231–243.
37. Perkins, S. J. (1986) Protein volumes and hydration effects. *Eur. J. Biochem. 157*, 169–180.
38. Tanford, C. (1961) Physical Chemistry of Macromolecules, John Wiley and Sons, New York.
39. Kuntz, I. D., and Kauzman, W. (1974) Hydration of Proteins and Polypeptides. *Adv. Protein Chem. 28*, 239–345.
40. Mabuchi, K. (1991) Heavy-meromyosin-decorated actin filaments: A simple method to preserve actin filaments for rotary shadowing. *J. Struct. Biol. 107*, 22–28.
41. Mabuchi, K. (1990) Melting of myosin and tropomyosin: Electron microscopic observations. *J. Struct. Biol. 103*, 249–256.
42. Grabarek, Z., and Gergely, J. (1990) Zero-length crosslinking procedure with the use of active esters. *Anal. Biochem. 185*, 131–135.
43. Arnold, K., Bordoli, L., Kopp, J., and Schwede, T. (2006) The SWISS-MODEL workspace: A web-based environment for protein structure homology modelling. *Bioinformatics 22*, 195–201.
44. Kopp, J., and Schwede, T. (2004) The SWISS-MODEL Repository of annotated three-dimensional protein structure homology models. *Nucleic Acids Res. 32*, D230–D234.
45. Schwede, T., Kopp, J., Guex, N., and Peitsch, M. C. (2003) SWISS-MODEL: An automated protein homology-modeling server. *Nucleic Acids Res. 31*, 3381–3385.
46. Guex, N., and Peitsch, M. C. (1997) SWISS-MODEL and the Swiss-PdbViewer: An environment for comparative protein modeling. *Electrophoresis 18*, 2714–2723.
47. Peitsch, M. C. (1995) Protein modeling by E-mail. *Bio/Technology 13*, 658–660.
48. Jones, T. A., Zou, J. Y., Cowan, S. W., and Kjeldgaard, M. (1991) Improved methods for building protein molecules in electron density maps and the location of errors in these models. *Acta Crystallogr. A47*, 110–119.
49. Brunger, A. T., Adams, P. D., Clore, G. M., Delano, W. L., Gros, P., Grosse-Kunstleve, R. W., Jiang, J.-S., Kuszewski, J., Nilges, M., Pannu, N. S., Read, R. J., Rice, L. M., Simonson, T., and Warren, G. L. (1998) Crystallography & NMR system. A new software suite for macromolecular structure determination. *Acta Crystallogr. D54*, 905–921.
50. Garcia De La Torre, J., Huertas, M. L., and Carrasco, B. (2000) Calculation of hydrodynamic properties of globular proteins from their atomic-level structure. *Biophys. J. 78*, 719–730.
51. Pearson, R. B., Ito, M., Morrice, N. A., Smith, A. J., Condron, R., Wettenhall, R. E., Kemp, B. E., and Hartshorne, D. J. (1991) Proteolytic cleavage sites in smooth muscle myosin-light-chain kinase and their relation to structural and regulatory domains. *Eur. J. Biochem. 200*, 723–730.
52. Padre, R. C., and Stull, J. T. (2000) Functional assembly of fragments from bisected smooth muscle myosin light chain kinase. *J. Biol. Chem. 275*, 26665–26673.
53. Numata, T., Katoh, T., and Yazawa, M. (2001) Functional Role of the C-Terminal Domain of Smooth Muscle Myosin Light Chain Kinase on the Phosphorylation of Smooth Muscle Myosin. *J. Biochem. 129*, 437–444.
54. Sobieszek, A. (1991) Regulation of smooth muscle myosin light chain kinase. Allosteric effects and co-operative activation by calmodulin. *J. Mol. Biol. 220*, 947–957 [erratum, (1991) *J. Mol. Biol. 222*, 1173].
55. Sobieszek, A., Strobl, A., Ortner, B., and Babiychuk, E. B. (1993) Ca^{2+}/calmodulin-dependent modification of smooth-muscle myosin light-chain kinase leading to its co-operative activation by calmodulin. *Biochem. J. 295*, 405–411.
56. Babiychuk, E. B., Babiychuk, V. S., and Sobieszek, A. (1995) Modulation of smooth muscle myosin light chain kinase activity by Ca^{2+}/calmodulin-dependent, oligomeric-type modifications. *Biochemistry 34*, 6366–6372.
57. Krueger, J. K., Olah, G. A., Rokop, S. E., Zhi, G., Stull, J. T., and Trewhella, J. (1997) Structures Of Calmodulin and a Functional Myosin Light Chain Kinase in the Activated Complex: A Neutron Scattering Study. *Biochemistry 36*, 6017–6023.
58. Politou, A. S., Gautel, M., Improta, S., Vangelista, L., and Pastore, A. (1996) The elastic I-band region of titin is assembled in a "modular" fashion by weakly interacting Ig-like domains. *J. Mol. Biol. 255*, 604–616.
59. Improta, S., Krueger, J. K., Gautel, M., Atkinson, R. A., Lefevre, J. F., Moulton, S., Trewhella, J., and Pastore, A. (1998) The assembly of immunoglobulin-like modules in titin: Implications for muscle elasticity. *J. Mol. Biol. 284*, 761–777.
60. Knighton, D. R., Pearson, R. B., Sowadski, J. M., Means, A. R., Ten, E. L., Taylor, S. S., and Kemp, B. E. (1992) Structural basis of the intrasteric regulation of myosin light chain kinases. *Science 258*, 130–135.
61. Knighton, D. R., Zheng, J. H., Ten Eyck, L. F., Ashford, V. A., Xuong, N. H., Taylor, S. S., and Sowadski, J. M. (1991) Crystal structure of the catalytic subunit of cyclic adenosine monophosphate-dependent protein kinase. *Science 253*, 407–414.
62. Knighton, D. R., Zheng, J. H., Ten Eyck, L. F., Xuong, N. H., Taylor, S. S., and Sowadski, J. M. (1991) Structure of a peptide inhibitor bound to the catalytic subunit of cyclic adenosine monophosphate-dependent protein kinase. *Science 253*, 414–420.
63. Hu, S. H., Parker, M. W., Lei, J. Y., Wilce, M., Benian, G. M., and Kemp, B. E. (1994) Insights into autoregulation from the crystal structure of twitchin kinase. *Nature 369*, 581–584.
64. Bork, P., Holm, L., and Sander, C. (1994) The immunoglobulin fold. Structural classification, sequence patterns and common core. *J. Mol. Biol. 242*, 309–320.
65. Mrosek, M., Labeit, D., Witt, S., Heerklotz, H., von Castelmur, E., Labeit, S., and Mayans, O. (2007) Molecular determinants for the recruitment of the ubiquitin-ligase MuRF-1 onto M-line titin. *FASEB J. 21*, 1383–1392.
66. Areschoug, T., Linse, S., Stalhammar-Carlemalm, M., Heden, L. O., and Lindahl, G. (2002) A proline-rich region with a highly periodic sequence in streptococcal β protein adopts the polyproline II structure and is exposed on the bacterial surface. *J. Bacteriol. 184*, 6376–6383.
67. Forbes, J. G., Jin, A. J., Ma, K., Gutierrez-Cruz, G., Tsai, W. L., and Wang, K. (2005) Titin PEVK segment: Charge-driven elasticity of the open and flexible polyampholyte. *J. Muscle Res. Cell Motil. 26*, 291–301.
68. Granzier, H. L., and Labeit, S. (2005) Titin and its associated proteins: The third myofilament system of the sarcomere. *Adv. Protein Chem. 71*, 89–119.
69. Nagy, A., Grama, L., Huber, T., Bianco, P., Trombitas, K., Granzier, H. L., and Kellermayer, M. S. (2005) Hierarchical extensibility in the PEVK domain of skeletal-muscle titin. *Biophys. J. 89*, 329–336.
70. Ma, K., Kan, L., and Wang, K. (2001) Polyproline II helix is a key structural motif of the elastic PEVK segment of titin. *Biochemistry 40*, 3427–3438.
71. Ma, K., and Wang, K. (2003) Malleable conformation of the elastic PEVK segment of titin: Non-cooperative interconversion of polyproline II helix, β-turn and unordered structures. *Biochem. J. 374*, 687–695.
72. Carrasco, B., and Garcia de la Torre, J. (1999) Hydrodynamic properties of rigid particles: Comparison of different modeling and computational procedures. *Biophys. J. 76*, 3044–3057.
73. Somlyo, A. P., Devine, C. E., Somlyo, A. V., and Rice, R. V. (1973) Filament organization in vertebrate smooth muscle. *Philos. Trans. R. Soc. London, Ser. B 265*, 223–229.
74. Gallagher, P. J., and Stull, J. T. (1997) Localization of an actin binding domain in smooth muscle myosin light chain kinase. *Mol. Cell. Biochem. 173*, 51–57.
75. Ye, L. H., Hayakawa, K., Kishi, H., Imamura, M., Nakamura, A., Okagaki, T., Takagi, T., Iwata, A., Tanaka, T., and Kohama, K. (1997) The structure and function of the actin-binding domain of myosin light chain kinase of smooth muscle. *J. Biol. Chem. 272*, 32182–32189.
76. Cross, R. A., and Sobieszek, A. (1985) Influence of smooth muscle myosin conformation on myosin light chain kinase binding and on phosphorylation. *FEBS Lett. 188*, 367–374.
77. Sobieszek, A. (1985) Phosphorylation reaction of vertebrate smooth muscle myosin: An enzyme kinetic analysis. *Biochemistry 24*, 1266–1274.
78. Ngai, P. K., and Walsh, M. P. (1987) Purification of smooth-muscle myosin free of calmodulin and myosin light-chain kinase. Susceptibility to oxidation. *Biochem. J. 246*, 205–211.
79. Hong, F., Haldeman, B. D., John, O. A., Brewer, P. D., Wu, Y. Y., Ni, S., Wilson, D. P., Walsh, M. P., Baker, J. E., and Cremo, C. R. (2009) Characterization of tightly associated smooth muscle myosin-myosin light-chain kinase-calmodulin complexes. *J. Mol. Biol. 390*, 879–892.
80. Granzier, H. L., and Labeit, S. (2004) The giant protein titin: A major player in myocardial mechanics, signaling, and disease. *Circ. Res. 94*, 284–295.
81. Fukuda, N., and Granzier, H. L. (2005) Titin/connectin-based modulation of the Frank-Starling mechanism of the heart. *J. Muscle Res. Cell Motil. 26*, 319–323.
82. Qin, X. R., Kurosaki, C., Yoshida, M., Hayashi, F., and Yokoyama, S. (2010) Solution structure of the fourth Ig-like domain from myosin light chain kinase, smooth muscle. (manuscript in preparation).
83. Kobe, B., Heierhorst, J., Feil, S. C., Parker, M. W., Benian, G. M., Weiss, K. R., and Kemp, B. E. (1996) Giant Protein Kinases−Domain

Interactions and Structural Basis of Autoregulation. *EMBO J. 15*, 6810–6821.
84. Mayans, O., van der Ven, P. F., Wilm, M., Mues, A., Young, P., Furst, D. O., Wilmanns, M., and Gautel, M. (1998) Structural basis for activation of the titin kinase domain during myofibrillogenesis. *Nature 395*, 863–869.
85. DeLano, W. L. (2002) The PyMOL Molecular Graphics System, DeLano Scientific, Palo Alto, CA.